Energy Strategy Reviews 47 (2023) 101094

Contents lists available at ScienceDirect

Energy Strategy Reviews

journal homepage: www.elsevier.com/locate/esr

Energy storage sizing for virtual inertia contribution based on ROCOF and local frequency dynamics

Dominique Alonso Sørensen [a,b,*], Daniel Vázquez Pombo [c,d], Esther Torres Iglesias [a]

[a] Department of Electrical Engineering, University of the Basque Country (UPV/EHU), Ingeniero Torres Quevedo Plaza, 1, Bilbao, 48013, Spain
[b] Grid Connection Department, Arteche, Derio Bidea 28, Munguia, 48100, Spain
[c] Department of Wind and Energy Systems, Technical University of Denmark (DTU), Frederikborsvej 399, Roskilde, 4000, Denmark
[d] R&D Strategic Development, Vattenfall AB, Evenemangsgatan 13C, Solna, 169 56, Sweden

ARTICLE INFO

Keywords:
Africa
Supercapacitor
BESS
FFR
Local inertia
Inertia distribution

ABSTRACT

Large integration of renewable energy sources has caused a dramatic reduction of inertia in modern power grids. Which has caused the development of virtual inertia techniques facilitating support from power electronic interfaced devices. In this paper, we consider traditionally dismissed phenomena such as local frequency dynamics in order to propose a methodology sizing the virtual inertia contribution requirements of energy storage systems. Such sizing considers: first, a given safety level defined in terms of maximum allowed rate of change of frequency (RoCoF) for the reference fault; and second the local area dynamics. This allows to distribute the inertia provision effort around the power system resulting in lower overall power and energy requirements for the energy storage. The validation is approached using the IEEE 9-bus system, then, the island of Santiago, Cape Verde is employed as a realistic study exploring its inertia needs. Such isolated system aims to reach 100% renewable energy in the next decades and yet, it has been stuck around 20% for the past 7 years due to instability concerns. Therefore, this system would strongly benefit from virtual inertia integration. The method proves to improve the frequency response not only of the overall system, but also of the individual areas.

1. Introduction

The global energy industry is shifting towards a low carbon economy. Among the different reasons, climate change, and uncertainties in the supply of gas and petrol, stand out as motivators behind the need of lowering the energy consumed by polluting and non-renewable sources [1]. Particularly in Africa, significant efforts focus on substituting conventional synchronous generation by increasing the penetration level of Power Electronic-Interfaced Renewable Energy Sources (PEIRES) [2]. Such replacement of conventional Synchronous Generators (SG) with PEIRES poses a number of other non-trivial challenges. In this context, it is of the utmost importance for these new units to contribute in terms of voltage and frequency control; which has motivated research such as the one from Ustun et al. [3] which focuses on improving load flow analysis to better account for the specific characteristics of PEIRES.

The inertia lost by replacing SG represents a rising concern for system stability growing along with the energy transition progress. Several recent events highlight the importance of these challenges such as, the blackout in South Australia in 2016; which was a consequence of a cascading failure ending up with the split of the Southern synchronous area into two different islands [4]. In fact, there are many cases reported in the literature such as the Danish–Swedish blackout in 2003, or the UK's blackout in 2019 [5].

While SGs provide a natural inertial response due to their electromagnetic coupling, PEIRES do not. Overcoming this limitation, the concept of Virtual Inertia (VI) was introduced in order to facilitate the displacement of SGs in favour of PEIRES. It consists on a control scheme emulating the SG kinetic energy response. Beck et al. [6] developed a strategy that allows inverter based generation to mimic the SG behaviour. This new configuration enables RES to contribute to frequency regulation and inertia support using two different approaches, either by curtailing RES in order to have regulation capability [7,8]; or by introducing Energy Storage System (ESS) capable of reacting based on frequency deviations [9]. According to Tarnowski et al. [10], WTs can provide an inertial response by extracting the kinetic energy stored at their rotational mass with approximate inertia constant of 3.5 s [11]. Nevertheless, WTs require power electronics sensitive to frequency

* Corresponding author.Department of Electrical Engineering, University of the Basque Country (UPV/EHU), Ingeniero Torres Quevedo Plaza 1, Bilbao 48013, Spain
E-mail address: dominique.alonso@arteche.com (D. Alonso Sørensen).

https://doi.org/10.1016/j.esr.2023.101094
Received 30 June 2022; Received in revised form 2 April 2023; Accepted 16 April 2023
Available online 3 May 2023

changes to allow WTs to adapt their power reference based on frequency measurements [12]. In this context, WT-droop control based on ROCOF is used for VI purposes [13]. In addition, WTs present a recovery period for the rotational speed appearing right after the inertia release which tends to cause a second frequency dip [14]. Such second dip is particularly dangerous as it damages frequency stability and cause unnecessary tripping of protective relays [15,16]. Therefore, ESS is the best candidate for providing VI and other frequency-related ancillary services, increasing system efficiency, enabling RES to produce at their maximum power point and decreasing frequency instability [7].

There are a number of publications available related to VI implementation with ESS support. For instance, in Knap et al. [17] study the feasibility of using a Lithium-ion BESS in a laboratory setup. Ud et al. [18] focused on ultra-capacitors, demonstrating their suitability and performance for load-frequency control. While Sigris et al. [19] discussed the effect of different control parameters on the frequency stability provided by ultra-capacitor. Other works explore ESS sizing such as in El-Bidairi et al. [20]. Particularly, this research presents the optimal size for VI and Fast Frequency Response (FFR) support of an ESS in an islanded microgrid focusing on the frequency stability. The optimum size is found based on parameters such as allowed frequency deviation and nadir. In [21], Knap et al. present the sizing problem formulation for a system with one area was based on the minimum required inertia and maximum ROCOF deviation. Once again, the authors neglected the contribution of different generation areas in the sizing approach, dismissing the effect of the frequency along the system. In contrast, Abubakr et al. [22] presented an adaptive load-frequency control taking into account the tie-line load flow in a two-area system. This presents an enhancement since the contribution of other generation areas are considered. Bera et al. [23] propose an optimization formulation based on probabilistic minimum inertia as a function of the loading factor and clearing time. All the reviewed articles consider a single machine equivalent model to represent the system in their sizing methods. Nevertheless, Machowski et al. [24] demonstrate how the local inertia can lead to severe frequency drops in systems with uneven inertia distribution. This can cause the tripping of the protection relay of the generators of the area with lowest inertia, which could initiate a cascade effect of generator‘s disconnection, causing a major issue similar to the aforementioned UK incident.

There are different technical advantages and disadvantages of different ESS technologies. For instance, the time of energy release, the charge/discharge number of cycles, etc. Akram et al. [25] propose a Hybrid Energy Storage System (HESS) which consists of having two types of technology for frequency regulation. The first is aiming for VI capability, whereas, the other one is to provide FFR support. The sizing formulation is once again based on minimum inertia requirement, in a single machine system.

Another problem that power systems are facing is local inertia. This phenomena manifests when different generation areas have uneven inertia distribution [26,27]. Their heterogeneity may cause RoCoF mismatches and in some cases to be out of the limits imposed by the system operators. This would lead to the activation of the Under-Frequency Load Shedding (UFLS).

The available literature discusses how sizing formulation considered limitations regarding RoCoF and nadir frequency. Other, more complex sizing formulation have also included the effects of ESS's time constants or the load's V-f dependency. Existing methods approach sizing with formulations considering the lumped effect of the overall system. Thus, disregarding the electrical distances among generating areas, and the inertia distribution, which might lead with surpassing the RoCoF threshold. Overcoming such limitations, this research proposes a VI-focused sizing methodology aiming to limit the RoCoF of every area in the system. This is done by distributing the VI scheme all along the system, which is advantageous since the local RoCoF is considered, and the frequency dynamics will be more homogeneous throughout the system. To compute the necessary inertia of a certain area, its local distribution, and the electrical distance from the reference fault location to the generation area are considered. Then, the computed VI requirement is then applied to the generating area. Thereafter, the fault location is changed in order to verify that the needed VI is enough for all location. The methodology is verified using the well known IEEE 9-bus system proving the suitability of the technique. Afterwards, the method is applied to the Island of Santiago in Cape Verde, Africa for two reasons. First, to highlight the usefulness of the method in a realistic study case of an isolated system striving for 100% renewable deployment. Second, to provide insight to the local system operator regarding the VI required to deal with the frequency instability that might appear considering the expected RES increase of over the following years.

The structure of the paper is as follows, Section 2 reviews different topics related to frequency dynamics in power systems after sudden power mismatch. Then, the sizing formulation is presented in Section 3, and validated against the 9-bus system, and with the Cape Verde Reference System (CVRS) which are presented in Section 4. The results of both study cases are presented in the subsections of the system modelling section. This is followed by a discussion of results in Section 5 along with a comparison of the results of both cases presented in this paper. Lastly, Section 6 concludes the paper.

2. Frequency in power systems

Frequency regulation relies on the correct balance between power supply and demand. At a system level, such balance is achieved by means of a natural Inertial Response (IR) and a three level hierarchic frequency control architecture as represented in Fig. 1. There, the different frequency recovery stages after a sudden generation loss are represented; where point A constitutes the moment where the frequency excursion takes place. Thereafter, IR and Fast Frequency Response (FFR), Primary Frequency Response (PFR) and Secondary Frequency Response (SFR) spawn between A to B, B to C, and C to D respectively. In the figure, B corresponds to the nadir frequency, and C corresponds to the moment when SFR is activated. This last stage is then deployed until the frequency is reestablished to the nominal value.

IR is uncontrollably provided by synchronous units due to the kinetic energy stored at their rotating masses. This response is in practice a dumping effect keeping the frequency around its nominal value. Once a frequency event occurs, IR, and FFR provide a time buffer until the system collapses or the power unbalance is corrected. Then, a minimum inertia reserve is required in order to allow the first control action aiming to minimize frequency excursions, Primary Frequency Response (PFR), to be activated. Due to its importance, transmission system operators establish limitations regarding maximum RoCoF, nadir frequency, and minimum inertia, but also the activation time and duration of the different control actions. For instance, according to different grid codes AEMO [28], Nordic [29], and EirGrid [30], the time frame range of PFR starts from a few seconds after a power unbalance up to 30 s. Subsequently, secondary frequency control (SFR) takes over by aiming to reestablish the frequency to the nominal value. This is followed by tertiary and subsequent control whose objective is to recover generation reserves.

Traditionally, the IR of a system could be computed simply by considering the lumped effect of all the generators of a system as:

$$RoCoF_{sys} = \frac{df_{sys}}{dt} = \frac{\Delta P \cdot f_n}{2 \cdot H_{sys}} \tag{1}$$

where $RoCoF_{sys}$ is often expressed as the rate of change of frequency at the centre of inertia ($RoCoF_{COI}$). Then, the frequency deviation Δf_{COI} of the centre of inertia is defined by Eq. (2), while the total system inertia (H_{sys}) is computed as per Eq. (3), where S_i is the rated power of the ith generator.

$$\Delta f_{COI} = \frac{\sum H_i \cdot \Delta f_i}{\sum H_i} \tag{2}$$

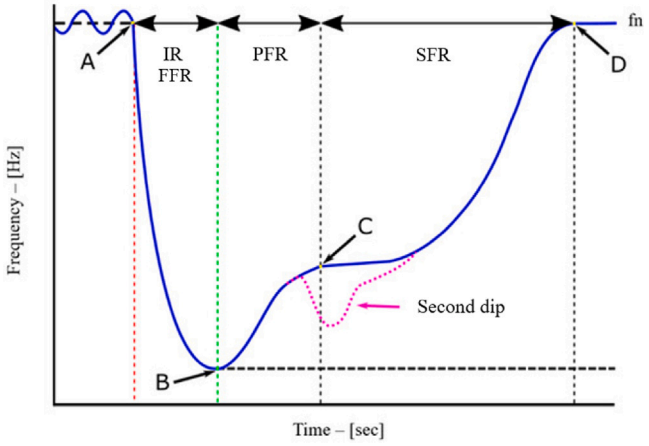

Fig. 1. Frequency response stages, reproduced from [16].

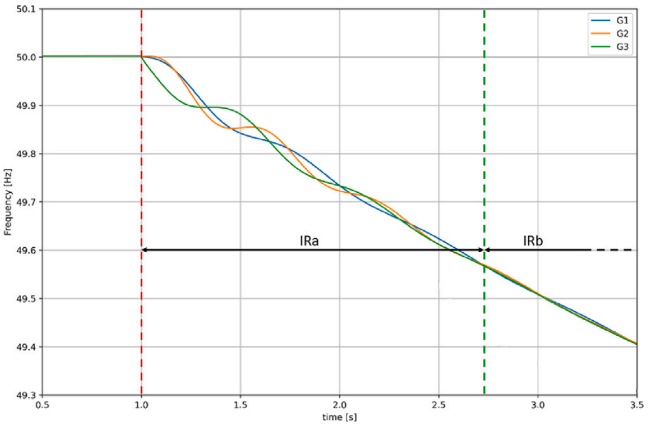

Fig. 2. Inertial response stages.

$$H_{sys} = \frac{\sum H_i \cdot S_i}{\sum S_i} \tag{3}$$

Nevertheless, IR can be divided into two different stages. A first stage (IRa) related to the rotor swing and local RoCoF; while the second (IRb) is related to the frequency drop after a sudden power unbalance. In this sense, IRa needs to consider the electrical distance between the fault location and the generator. Therefore, to compute the RoCoF of a specific area, the equivalent impedance has to be considered. Also note, that FFR and VI act during the same timeframe as IR, respectively focusing on limiting nadir and RoCoF. Thus, resulting complementary.

In Fig. 2 it is easy to view the aforementioned stages. The first second present the rotor swing of the SG of the different areas. IRb is related with Eq. (6), and (7).

For illustration purposes, we present the case of two parallel generators connected by means of a transmission line in Fig. 3. In such system, the local frequency deviation, and the step load are calculated as per eq (4), which can be generalized for a multi-machine system by introducing df_{sys}/dt as in eq (5) [24]:

$$\frac{df_l}{dt} = \frac{H_{sys}}{H_l} \cdot \frac{X_{sys}}{X'_d + X_T} \cdot \frac{df_{sys}}{dt} \tag{4}$$

$$\frac{df_l}{dt} = \frac{1}{H_l} \cdot \frac{X_{sys}}{X'_d + X_T} \cdot \frac{\Delta P \cdot f_n}{2} \tag{5}$$

Where $\frac{df_l}{dt}$ stands for the local RoCoF, while H_{sys} and H_l do so for the system and the local inertia constants respectively. Then, X_{sys}, X'_d, and X_T respectively represent the system equivalent reactance, the

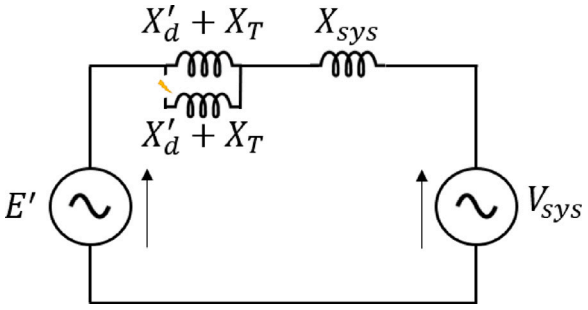

Fig. 3. Equivalent circuit of parallel generators connected to an infinite bus.

generator transient reactance, and the reactance of the transformer. Eq. (5) shows that the greater the ratio between the system inertia H_{sys} and the local inertia H_l, the higher is the local RoCoF, which means that the generator slows down faster. Then, from Eq. (4) it is clear that the electrical distance is proportional to the RoCoF. Lastly, X_{sys_a} represents the equivalent impedance from the fault location to the area of interest. During IRb, the power mismatch of every generation area is compensated based on their inertia constants. In such situation, RoCoF is assumed uniform for all generators. Thus, allowing to substitute the swing equation into Eq. (6) resulting into Eq. (7).

$$\frac{d\Delta f_1}{dt} \approx \frac{d\Delta f_2}{dt} \approx \frac{d\Delta f_n}{dt} \tag{6}$$

$$\frac{\Delta P_1}{H_1} \approx \frac{\Delta P_2}{H_2} \approx \frac{\Delta P_i}{H_i} \tag{7}$$

Now, the relationship between system and local inertia can be expressed as Eq. (8), which states the contribution of each generation area during IRb. Once again, a larger system to local inertia ratio implies lower contribution from the considered generation area.

$$\Delta P_l = \frac{H_l}{H_l + H_{sys}} \cdot \Delta P \tag{8}$$

Eq. (8) states the contribution of each generation area to cover the step load. Again, the ratio between the local and system inertia has a significant impact on the contribution of each area to the overall system. Note that, according to Eq. (8), the larger is the ratio of system to local inertia, the lower will be its contribution to compensate for the step load. Therefore, its impact might be lower.

As presented in Eq. (9), PFR acts based on the droop characteristics introducing a frequency error (Δf) which needs to be corrected by SFR.

$$R = \frac{\Delta f}{\Delta P} \tag{9}$$

From the ESS perspective, two points must be addressed. First, the electrical distance from the different generation areas must limit local RoCof as per Eq. (4). Another key consideration is keeping the system to local inertia ratio as small as possible to achieve a more homogeneous RoCoF distribution, potentially avoiding generator trips and the eventual systemic collapse.

For demonstration purposes, a generic ESS for VI support is introduced in the IEEE 9-bus system [31]. Particularly, in the area with the lowest inertia. The frequency event trigger is introduced as a perturbation ΔP integrated at the three different loads at each case. In this way, it is possible to demonstrate how the RoCoF behaves differently depending on its location, given the uneven inertia distribution. To begin with, the perturbation is assumed at the closest location to the VI scheme; which is then placed upon the furthest in a second calculation round.

Fig. 4 represents the expected RoCoF after an outage of 35 MW (9% of the load base) in the different areas. The VI scheme is placed at area 2, the one with lowest inertia. The simulation number corresponds

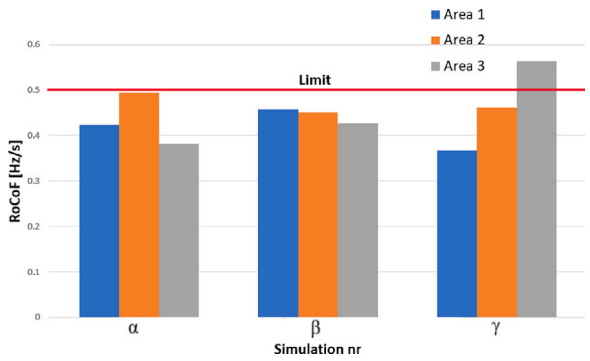

Fig. 4. Location impact on RoCoF.

with the outage place. Simulation 1 is the outage of the closest point to the VI placement. Simulation 2 corresponds to the second closest area which is area 1. Area 1 represents the place with the highest inertia of the system. Area 3 is the furthest area to the VI placement. The results highlight how the perturbation location has a great impact on the RoCoF value. Another aspect to consider is that the closest is the perturbation to the area with the highest inertia, the less the frequency swings. The results highlight the need for a system with more homogeneous inertia distribution.

3. Sizing of virtual inertia storage scheme

The existing methodologies aiming to size ESS based on limiting ROCOF and nadir frequency employ single machine equivalent systems. However, this approach results over simplistic once the local inertia distribution is considered since it is sufficient for single-machine systems to limit the RoCoF. Which, in turn, may cause local frequency dynamics to trigger a cascading protection activation starting with the UFLS of a generator. Therefore, to deal with this problematic, the VI support must consider the inertia distribution, and the electrical distances all along the system; which will influence inverter power and VI constants in order to consider each area's individual needs. The following methodology has been applied to estimate the inertia required to limit the rate of change of frequency (RoCoF) to a desired value. The swing equation (Eq. (1)) is used to estimate the required inertia. This value is then used to determine the inertia provision capacity of the energy storage system (ESS) using Eq. (11). This equation takes into account both the required inertia for the ith area (H_{req_i}) and the actual inertia of the ith area (H_{area_i}). It is important to note that an area only requires additional inertia to limit the RoCoF to the desired value when $H_{req_i} > H_{area_i}$.

$$H_{req_i} = \frac{1}{df_l/dt} \cdot \frac{X_{sys}}{X'_d + X_T} \cdot \frac{\Delta P \cdot f_n}{2} \tag{10}$$

$$H_{ESS_i} = H_{req_i} - H_{area_i} \tag{11}$$

The proposed method goes beyond the utilization of the swing equation considering the lumped effect on the system. Hence, the swing equation is modified so that the electrical distances are considered. In this regard, the required H_{ESS} contribution must be obtained for each area in order to ensure the RoCoF requirement to be fulfilled in the whole power system. Then, the proposed methodology is presented (see Fig. 5).

The methodology outlined above enables us to calculate the required inertia to ensure that the RoCoF remains within the desired limits. To relate the necessary energy from the ESS with the required inertia, we follow the next step:

$$H_{req_i} = H_{ESS_i} + H_{area_i} = \frac{\sum H_i \cdot S_i + k_{VI_i} \cdot S_{ESS_i}}{\sum S_i} \tag{12}$$

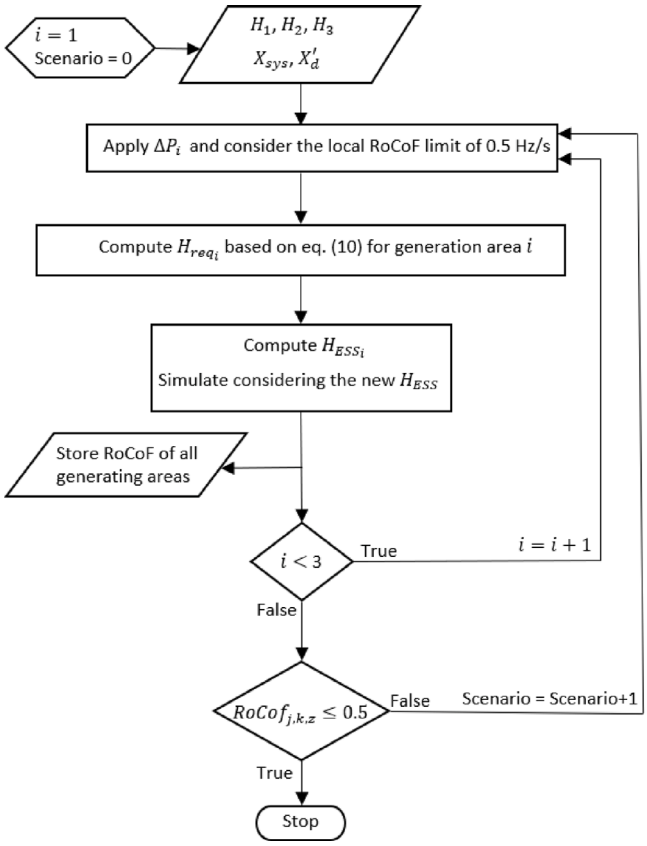

Fig. 5. Flowchart of the applied methodology.

This equation establishes the relationship between the energy required to limit the RoCoF, the actual kinetic energy produced by the synchronous generator, and the required energy coming from the ESS with VI capabilities.

Once we have determined the required energy, we can increase the virtual inertia gain while maintaining the relationship with the energy needed from the ESS that was previously calculated. With the new value of K_{VI} and the known energy, we can calculate the rated power of the inverters using the equation $S_{ESS_i} = \frac{Energy_{needed}}{k_{VI_i}}$. By considering the iterative virtual inertia gain that gives the desired RoCoF limit, we can ensure that the system operates within the required parameters.

Furthermore, it is noteworthy that this methodology can be applied in lower levels of the power system, for instance enabling to calculate the necessary VI support of each RES unit, or of particular branches in radial systems. This can homogenize the system so that the local frequencies are diminishing its impact.

4. Case studies: modelling and results

In this section, we evaluate the efficacy of the proposed methodology in two different study cases. The selected software evaluating methodology is enabled by the simulation tool DigSilent PowerFactory v2022. Case A validates the methodology by employing the well known IEEE 9-bus system presented in [31]. Subsequently, Case B showcases the usefulness of the methodology by applying it to the Cape Verde Reference System (CVRS) [32]. Which presents a real isolated system with 13% of RES integration in deer need of integrating VI schemes.

Note that, the design criteria is based on the RoCoF limits proposed by different system operators, summarized in Table 1. Therefore, we chose the most restrictive value of 0.5 Hz/s as the target RoCoF. Since the ROCOF is calculated as the first derivative of frequency, small

Table 1
System operator requirements [28–30].

	AEMO	Nordic	EirGrid
Nadir frequency	47.6	48.85	48.85
RoCoF	1.5 Hz/s	0.5 Hz/s	1 Hz/s

Table 2
Change in electrical distances between areas.

	Old value [Ω]	New value [Ω]	% difference
X_{L21}	130.134	11.23	91.37
X_{L13}	138.589	65	53.10
X_{L32}	91.411	91.411	0

variations in the measurement interval can lead to errors in the ROCOF value. To mitigate this issue, we set the time interval (dt) for frequency measurement to 200 ms [33] in our study, in order to accurately capture and analyse changes in frequency over time

The VI scheme integrated in the two study cases is the so-called continuous df/dt controller [34]. The continuous control is integrated into the active power control block of an ESS. Fig. 6 illustrates a simplified representation of one of the generation areas. As shown in the figure, the power generated by the synchronous generator does not take into account turbine-governor control and primary or secondary frequency control. This is because the focus of this research is on the first few hundred milliseconds, during which time the turbine-governor response does not significantly affect the behaviour of the synchronous generator beyond its intrinsic inertia. Within the red box in the figure, the virtual inertia control scheme can be found. This scheme involves filtering the derivative of the frequency with T=0.05 and multiplying it by the virtual inertia gain, which is calculated using the methodology described in this article. The time-frame of interest in this paper is the first hundreds of milliseconds. Therefore, the PFR control loop is not considered at the SG since it does not affect the results rather than the inertial response.

4.1. Case A: IEEE 9-bus system results

The IEEE 9-bus system, depicted in Fig. 7, has been slightly modified by worsening the inertia distribution of each generation area in order to better showcase the relevance of the proposed method. Table 2 presents the modification of the line lengths between the different generation areas. Hence, generation areas 1, and 2 are close to each other, and far from generation area 3. The kinetic energy of the different areas is presented in Table 4. Areas 1, 2, and 3 store of 880 MWs, 420 MWs, and 418 MWs, respectively. This shows that the Area 1 is the greatest area among the system in terms of inertia constant and rated power, please refer to Table 3, which means that the delivered power from this area will be greater than the rest. Regarding RoCoF, it might present more stable values considering the fault location. Then, the total system inertia is 4.09 s while the local values can be computed using Eq. (3); resulting in 2.09 s, 1 s, and 0.995 s, respectively for each generating area.

This modified version of the IEEE 9-bus system is then used to compute three different scenarios coping with a limitation of 0.5 Hz/s, after a sudden load increase of 35 MW at each node. Scenario 0 represents the base case, in which VI support is not integrated into the system.

To evaluate the superiority of the proposed method, three different scenarios are considered when responding to a step load of 35 MW in each generating area. In Scenario 0 no VI support in considered. Then, Scenario 1 integrates VI support calculating H_{ESS} using only area 1. While, Scenario 2 uses the full formulation to compute the required inertia for each area as H_{ESS_i}. Lastly, each scenario is evaluated three times, α, β, γ, by varying the step load implementation solely to areas 1, 2, and 3, respectively.

Table 3
Case A: Generators' input data.

		Area 1	Area 2	Area 3
New values	H [s]	5.5	2.8	3.8
	S [MVA]	160	150	110
Old values	H [s]	9.55	3.9	2.76
	S [MVA]	247.5	192	128

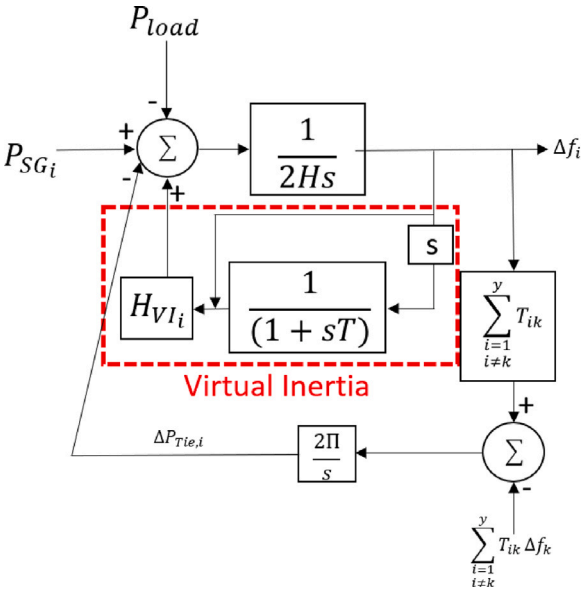

Fig. 6. Dynamic Model of generation area-i.

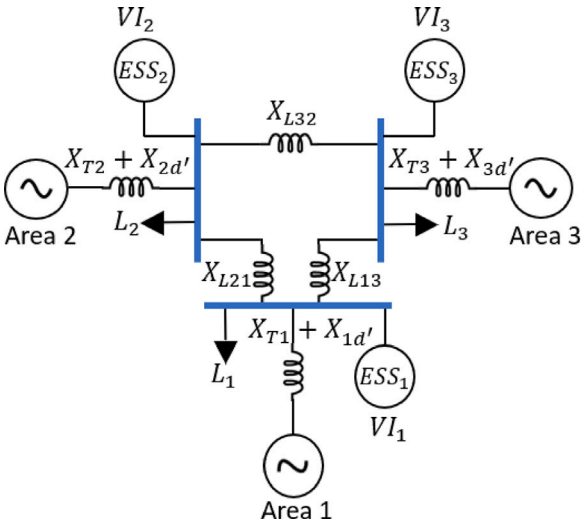

Fig. 7. Single Line Diagram IEEE-bus system.

The resulting RoCoF values of Scenario 0 for each area are presented in Fig. 8, where variations appear depending on the step load location. The results demonstrate that the desired RoCoF limits are violated at all locations for load steps of 35MW (9%). Therefore, in Scenario 1, the proposed methodology is applied to support VI considering the fault in area 1, whose results are presented in Fig. 9. Then, only α and γ satisfy the criteria; thus, making necessary to run Scenario 2 focusing on satisfying the VI needs of area 2 as shown in Fig. 10. Note that, α, β, and γ are simply iterations of the proposed methodology. Hence, Case A allows to conclude on the importance of considering local inertia phenomena by relocating the fault to all areas in the

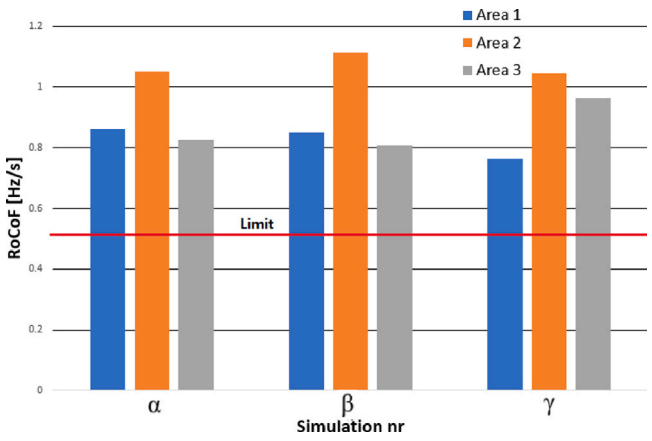

Fig. 8. Results for Case A and Scenario 0, base case without VI support.

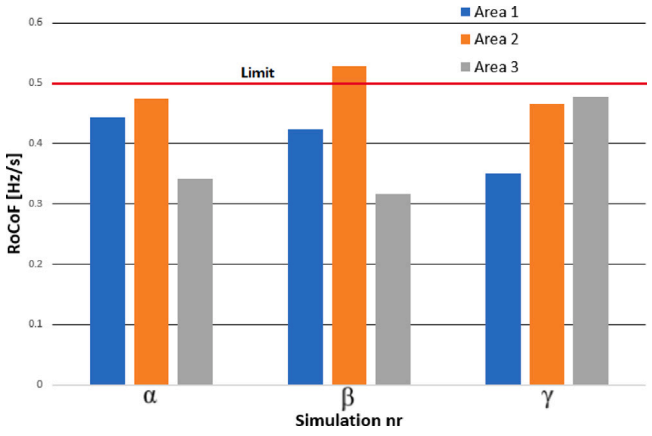

Fig. 9. Results for Case A and Scenario 1.

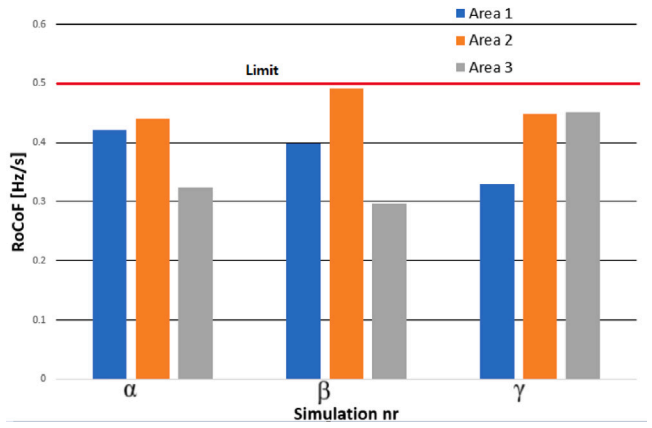

Fig. 10. Results for Case A and Scenario 2.

considered system in order to satisfy the RoCoF limit design criteria. Ultimately, by satisfying the criteria for the worst area (in this case 2), the RoCoF of all areas is improved, further ensuring safe operation.

The final results for the required ESS with VI are presented in Table 4. The converter for generation area 1 should have at least 1% of the total base power. The total energy capacity is 0.36%. The VI converter of area 2 is the biggest in capacity and converter size. In this case, the inverter rated power is of 4.52%, and the total energy capacity is 8.26%. The last area, represent 2.14% of rated power and a energy capacity of 1.8% of the total energy stored.

Table 4
IEEE 9-bus system final input data.

		Area 1	Area 2	Area 3
SG	H [s]	5.5	2.8	3.8
	S [MVA]	160	150	110
	Energy [MVA s]	880	420	418
VI	H [s]	1.5	7.5	3.5
	S [MVA]	4.2	19	9
	Energy [MVA s]	6.3	142.5	31.5
Total	H [s]	2.110	1.339	1.071

The methodology can be applied for any RoCoF limit and considering different power unbalances. The system inertia constant has increased from 4.09 s to 4.52 s with the integration of ESS with VI support. The results comparison, considering the previous case to the scenario where VI has been integrated demonstrates how the system is significantly enhanced. The virtual inertia (H) is calculated using Eq. (3). The numerator of this equation is based on the energy capacity of the system, while the denominator is based on the rated inverter power. This calculation allows us to estimate the virtual inertia of the system and determine whether it is sufficient to meet the desired RoCoF limit.

4.2. Case B: CVRS results

In order to highlight the usefulness of the proposed methodology, we have selected the African archipelago of Cape Verde as study case. The local government aims to reach 50% renewable by 2030 and 100% by 2050. In fact, a recent studies show how it would be possible to reach it far sooner [35,36]. However, due to stability issues the system operator has limited instantaneous renewable penetration at around 20%.

The focus of this study case is on the island of Santiago, the largest in the country, as it represents more than half the overall energy demands. Depicted in Fig. 11, the system is powered by 99 MW of fossil fuelled generators, and 13 MW of RES (combining wind and solar), although the peak load rarely exceeds 40 MW. The interested reader is referred to the open access Cape Verde Reference System [32].

Similar to the IEEE 9-bus system, the CVRS presents three generation areas as depicted in Fig. 11. Nevertheless, the configuration is slightly different. For instance, generation Area 3 is currently composed only of RES with no inertia support. Area 1 is by far the largest generation area in terms of power supply.

The remaining of the section is focused on testing the proposed methodology to size the required VI support satisfying the needs of every generation area. As in the previous case, a step load is introduced in each area to create three different scenarios. The total consumption assumed is 45 MW, and the step load increase is of 5 MW, thus representing 11% of power variation. Fig. 12, which presents the results for the CVRS without any VI support, shows the large degree of RoCoF variation; well above the design limit of 0.5 Hz/s. This is due to the high RES penetration level of the island and its very low inertia. Therefore, VI schemes should be deployed for all three generating areas.

The results of scenario 2 are presented in Fig. 13, which shows that RoCoF can be kept below the limit for all cases. Nevertheless, there are huge differences among cases, which is caused by the uneven inertia distribution of the system. Clearly, this behaviour can be improved with a coordinated VI support.

In summary, area 1 requires an ESS with a rated power of 4 MW or about 8% of the total base power. Area 2 has the largest capacity rating while requiring 12% of the base power. Lastly, area 3 is designed with a power level of 13% (see Table 5).

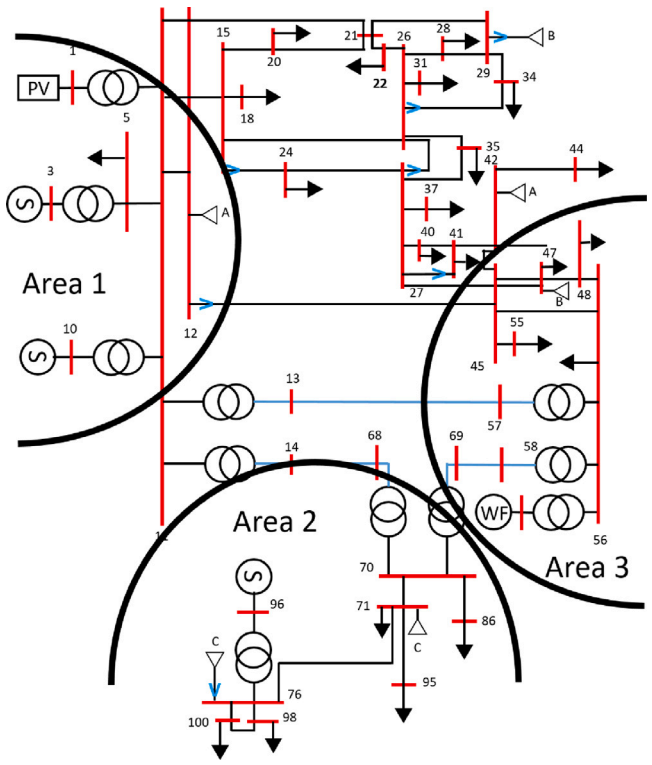

Fig. 11. Single line diagram of Santiago's simplified system.
Source: Reproduced from [32].

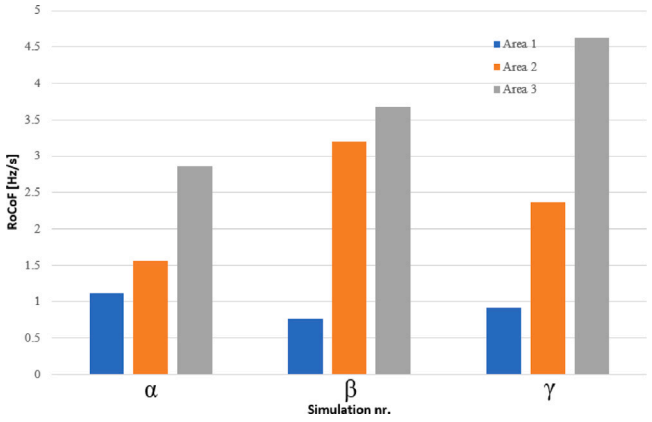

Fig. 12. Results for Case B and Scenario 1.

5. Discussion

This section aims to compare Cases A and B. Furthermore, the implications of electricity markets on the results are covered.

Neither case originally complied with the RoCoF design criteria of 0.5 Hz/s, which justified the need of introducing VI. However, Case A presented a more evenly distributed inertia, as demonstrated in Fig. 8. In fact, it can be seen that differences in homogeneity distribution are not significant when comparing them, for instance to Fig. 12.

Considering the inertia constants of each system. Case A have a system inertia of 4.52s and, Case B 3.5s. Both systems present almost the same ΔP. The main difference between both systems is the electrical distances. Since Case A is presented as a big system in terms of electrical distances, Case B is a small isolated power system.

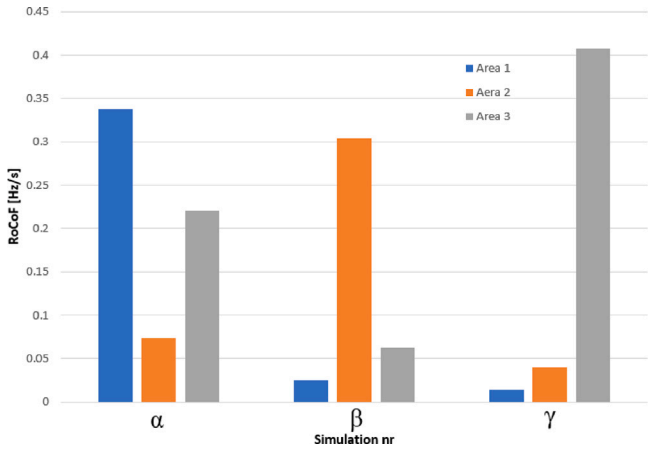

Fig. 13. Results for Case B and Scenario 2.

Table 5
Scenario 1,2 of the CVRS system.

		Area 1	Area 2	Area 3
SG	H [s]	3.5	2	0
	S [MVA]	25	10	15
	Energy [MVA s]	87.5	20	0
VI	H [s]	1	3	7
	S [MVA]	4	6	6.5
	Energy [MVA s]	4	18	45.5
Total	H [s]	1.83	0.76	0.91

5.1. Upcoming flexibility and inertia markets

The sizing methodology covered in this research focuses on ensuring the safe operation of the power system. Particularly, the resulting storage capacity corresponds to a minimum size satisfying the requirements. Therefore, the assumed perspective is that of a vertically integrated power system lacking a competitive energy market, as is the case of many African countries such as Cape Verde. However, regions such as the UK or the Nordics are starting to include inertial-like products into their markets, which justifies considering the profitability opportunities for ESS [37].

In the case of the UK, National Grid ESO is in the process of rolling out a new grid code. Among other novelties, the creation of an inertia market is envisioned with the particularity of allowing grid-forming devices to participate [38]. In the Nordics (Denmark, Norway, and Sweden) an FFR market is in operation since 2021. The regulations are generic to allow any capable unit to participate disregarding the specific technology [39]. While the medium to long term profitability of these markets remains unclear, at the moment they appear to be the most profitable option for ESS [40].

Clearly, participating in these and other similar markets will affect the sizing strategy of ESS. However, it is not possible to know at the moment which one (system security or market participation) will be the toughest constraint. Furthermore, a market-focused ESS sizer must acknowledge the broad diversity of products that could be offered these devices, thus falling out of the scope of this work. In such a context, the methodology developed in Section 3 could be integrated in the form of constraints.

6. Conclusions

The loss of the system inertia is an increasing concern in modern power systems due to the increasing integration of RES. The installation of energy storage or synchronous condensers are common practices aiming to enhance the stability. Different methods based on power

curtailment of RES or ESS have demonstrated their feasibility for VI support. Nevertheless, curtailment incurs in economic losses due to the loss of opportunity, and as it demands over installation, which makes ESS the preferred choice.

In this work, an ESS sizing process in terms of its VI contribution is proposed. The methodology estimates the inertia required to avoid reaching a certain nadir based on the role of local frequency dynamics and electrical distance between the fault location and any given area. In this context, the RoCoF of local areas defines the maximum allowed threshold for the reference fault. Therefore ensuring that the power system will survive the design event long enough for PFR to be activated. Furthermore, by considering the local inertia effects it is possible to ensure the robust operation of each part and the overall system.

The results point towards the suitability of this method to limit local RoCoF. The validation was undergone using the IEEE 9-bus system considering the extensive works related to frequency stability that can be found at the literature. Afterwards, a study case was presented using the CVRS for the island of Santiago in Cape Verde, Africa. The results showcase the many benefits of placing distributed VI schemes along the system. Hence, the proposed method is interesting from the system operator planning perspective, as it allows to ensure reliable operation based on frequency stability criteria.

This work could be continued by integrating the proposed methodology into an optimal ESS sizer accounting for participation in markets such us inertia, FFR, or FCR besides the classical day-ahead and reserve. In addition, virtual inertia gain may be adjusted based on different system operating conditions. Such measures aim to minimize the energy use by the ESS.

CRediT authorship contribution statement

Dominique Alonso Sørensen: Conceptualization, Methodology, Software, Validation, Writing – original draft, Visualization, Supervision. **Daniel Vázquez Pombo:** Validation, Formal analysis, Resources, Data curation, Writing – original draft, Visualization. **Esther Torres Iglesias:** Supervision, Methodology, Resources.

Declaration of competing interest

The authors declare that they have no known competing financial interests or personal relationships that could have appeared to influence the work reported in this paper.

Data availability

Data will be made available on request.

Acknowledgements

This research has been supported by the Basque Government, Spain (GISEL research group IT1191-19) and the UPV/EHU (GISEL research group 18/181). We would also like to express our appreciation to the R&D and Business Development Departments in Arteche Group for their generous funding and support of this research.

Appendix A. Supplementary data

Supplementary data to this article related to the system of Santiago, Cape Verde can be found online at 10.11583/DTU.17430413.

References

[1] T. Kåberger, Progress of renewable electricity replacing fossil fuels, Glob. Energy Interconnect. 1 (1) (2018) 48–52.
[2] G. Mutezo, J. Mulopo, A review of Africa's transition from fossil fuels to renewable energy using circular economy principles, Renew. Sustain. Energy Rev. 137 (2021) 110609.
[3] T.S. Ustun, Y. Aoto, Analysis of smart inverter's impact on the distribution network operation, IEEE Access 7 (2019) 9790–9804.
[4] Australian Energy Market Operator, Black System South Australia 28 September 2016, Australian Energy Market Operator, 2017.
[5] Y.-K. Wu, S.M. Chang, Y.-L. Hu, Literature review of power system blackouts, Energy Procedia 141 (2017) 428–431.
[6] H.-P. Beck, R. Hesse, Virtual synchronous machine, in: 2007 9th International Conference on Electrical Power Quality and Utilisation, 2007, pp. 1–6.
[7] P. Tielens, D. Van Hertem, Grid inertia and frequency control in power systems with high penetration of renewables, in: Young Researchers Symposium in Electrical Power Engineering, Date: 2012/04/16-2012/04/17, Location: Delft, the Netherlands, 2012.
[8] H. Xin, Y. Liu, Z. Wang, D. Gan, T. Yang, A new frequency regulation strategy for photovoltaic systems without energy storage, IEEE Trans. Sustain. Energy 4 (4) (2013) 985–993.
[9] G. Delille, B. Francois, G. Malarange, Dynamic frequency control support by energy storage to reduce the impact of wind and solar generation on isolated power system's inertia, IEEE Trans. Sustain. Energy 3 (4) (2012) 931–939.
[10] G.C. Tarnowski, P.C. Kjar, P.E. Sorensen, J. Ostergaard, Variable speed wind turbines capability for temporary over-production, in: 2009 IEEE Power & Energy Society General Meeting, IEEE, 2009, pp. 1–7.
[11] A. Žertek, G. Verbič, M. Pantoš, Participation of DFIG wind turbines in frequency control ancillary service by optimized rotational kinetic energy, in: 2010 7th International Conference on the European Energy Market, IEEE, 2010, pp. 1–6.
[12] X. Yingcheng, T. Nengling, Review of contribution to frequency control through variable speed wind turbine, Renew. Energy 36 (6) (2011) 1671–1677.
[13] W. Binbing, X. Abuduwayiti, C. Yuxi, T. Yizhi, RoCoF droop control of PMSG-based wind turbines for system inertia response rapidly, IEEE Access 8 (2020) 181154–181162.
[14] P.W. Christensen, G.C. Tarnowski, Inertia for wind power plants. State of the art review: Year 2011, 2011.
[15] J. Van de Vyver, J.D. De Kooning, B. Meersman, L. Vandevelde, T.L. Vandoorn, Droop control as an alternative inertial response strategy for the synthetic inertia on wind turbines, IEEE Trans. Power Syst. 31 (2) (2015) 1129–1138.
[16] D.V. Pombo, F. Iov, D.I. Stroe, A novel control architecture for hybrid power plants to provide coordinated frequency reserves, Energies 12 (5) (2019) 919.
[17] V. Knap, R. Sinha, M. Swierczynski, D.-I. Stroe, S. Chaudhary, Grid inertial response with lithium-ion battery energy storage systems, in: 2014 IEEE 23rd International Symposium on Industrial Electronics, ISIE, IEEE, 2014, pp. 1817–1822.
[18] M. ud din Mufti, S.A. Lone, S.J. Iqbal, M. Ahmad, M. Ismail, Super-capacitor based energy storage system for improved load frequency control, Electr. Power Syst. Res. 79 (1) (2009) 226–233.
[19] L. Sigrist, I. Egido, E.L. Miguélez, L. Rouco, Sizing and controller setting of ultracapacitors for frequency stability enhancement of small isolated power systems, IEEE Trans. Power Syst. 30 (4) (2014) 2130–2138.
[20] K.S. El-Bidairi, H.D. Nguyen, T.S. Mahmoud, S. Jayasinghe, J.M. Guerrero, Optimal sizing of battery energy storage systems for dynamic frequency control in an islanded microgrid: A case study of Flinders Island, Australia, Energy 195 (2020) 117059.
[21] V. Knap, S.K. Chaudhary, D.-I. Stroe, M. Swierczynski, B.-I. Craciun, R. Teodorescu, Sizing of an energy storage system for grid inertial response and primary frequency reserve, IEEE Trans. Power Syst. 31 (5) (2015) 3447–3456.
[22] H. Abubakr, J.M. Guerrero, J.C. Vasquez, T.H. Mohamed, K. Mahmoud, M.M. Darwish, Y.A. Dahab, Adaptive LFC incorporating modified virtual rotor to regulate frequency and tie-line power flow in multi-area microgrids, IEEE Access (2022).
[23] A. Bera, M. Abdelmalak, S. Alzahrani, M. Benidris, J. Mitra, Sizing of energy storage systems for grid inertial response, in: 2020 IEEE Power & Energy Society General Meeting, PESGM, IEEE, 2020, pp. 1–5.
[24] J. Machowski, Z. Lubosny, J.W. Bialek, J.R. Bumby, Power System Dynamics: Stability and Control, John Wiley & Sons, 2020.
[25] U. Akram, N. Mithulananthan, R. Shah, S.A. Pourmousavi, Sizing HESS as inertial and primary frequency reserve in low inertia power system, IET Renew. Power Gener. 15 (1) (2021) 99–113.
[26] B.A. Osbouei, G.A. Taylor, O. Bronckart, J. Maricq, M. Bradley, Impact of inertia distribution on power system stability and operation, in: 2019 IEEE Milan PowerTech, IEEE, 2019, pp. 1–6.
[27] D. Doheny, M. Conlon, Investigation into the local nature of rate of change of frequency in electrical power systems, in: 2017 52nd International Universities Power Engineering Conference, UPEC, IEEE, 2017, pp. 1–6.
[28] A.E.M. Operator, International Review of Frequency Control Adaptation, Tech. Rep2016, 2016.

[29] E. Ørum, M. Kuivaniemi, M. Laasonen, A.I. Bruseth, E.A. Jansson, A. Danell, K. Elkington, N. Modig, Future system inertia, ENTSOE, Brussels, Tech. Rep, 2015, pp. 1–58.
[30] EirGrid, DS3: RoCoF Workstream Plan, Tech. Rep 2014, 2014.
[31] P.M. Anderson, Power System Control and Stability: Vol. I., Science Press, 1977.
[32] D.V. Pombo, H.T. Nguyen, L. Chebbo, D.A. Sørensen, A multipurpose reference system based on the hybrid power grid of Cape Verde, IEEE Trans. Smart Grid (2022) 1.
[33] M. Rezkalla, A. Zecchino, S. Martinenas, A.M. Prostejovsky, M. Marinelli, Comparison between synthetic inertia and fast frequency containment control based on single phase EVs in a microgrid, Appl. Energy 210 (2018) 764–775.
[34] F. Gonzalez-Longatt, E. Chikuni, W. Stemmet, K. Folly, Effects of the synthetic inertia from wind power on the total system inertia after a frequency disturbance, in: IEEE Power and Energy Society Conference and Exposition in Africa: Intelligent Grid Integration of Renewable Energy Resources (PowerAfrica), 2012, pp. 1–7.
[35] D.V. Pombo, J. Martinez-Rico, H.M. Marczinkowski, Towards 100% renewable islands in 2040 via generation expansion planning: The case of São Vicente, Cape Verde, Appl. Energy 315 (2022) 118869.
[36] D.V. Pombo, J.M. Rico, S.V. Spataru, H.W. Bindner, P.E. Sørensen, Decarbonizing energy islands with flexibility-enabling planning: The case of Santiago, Cape Verde, Renew. Sustain. Energy Rev. (2023).
[37] Future of Balancing Services, Electricity System Operator Markets Roadmap, Tech. Rep, National Grid ESO, 2022, p. 93.
[38] A. Johnson, Grid Code GC0137: Minimum Specification Required for Provision of GB Grid Forming Capability (Formerly Virtual Synchronous Machine Capability), Tech. Rep, National Grid ESO, 2022, p. 10.
[39] ENTSO-E, Fast Frequency Reserve – Solution to the Nordic Inertia Challenge, Tech. Rep, European Network of Transmission System Operators for Electricity, 2019, p. 22.
[40] S. Kraftnät, Mimer, medelpris EUR/MW för avropad kapacitet för FCR-n, FCR-d upp och FCR-d ned för svenska och danska BA (average price EUR/MW for requested capacity for FCR-n, FCR-d up and FCR-d down for Swedish and Danish BA), 2022, https://mimer.svk.se/PrimaryRegulation/PrimaryRegulationIndex. (Accessed 14 December 2022).